Int. J. Electrochem. Sci., 8 **(2013)** 1189 - 1208

International Journal of
ELECTROCHEMICAL
SCIENCE
www.electrochemsci.org

Effect of KOH Concentration on the Oxygen Reduction Kinetics Catalyzed by Heat-Treated Co-Pyridine/C Electrocatalysts

Jinli Qiao[*], *Li Xu, Lei Ding, Penghui Shi, Lei Zhang, Ryan Baker, Jiujun Zhang*

[1] College of Environmental Science and Engineering, Donghua University, 2999 Ren'min North Road, Shanghai 201620, P. R. China
[2] National Research Council Canada, 4250 Wesbrook Mall Vancouver, BC, Canada V6T 1W5
[*]E-mail: qiaojl@dhu.edu.cn

Received: 17 November 2012 / *Accepted:* 14 December 2012 / *Published:* 1 January 2013

Using a simple thermal method, a non-noble metal electrocatalyst (Co-N-S/C) is successfully synthesized and its' composition is analyzed using EDX. The electrochemical activity of such a catalyst is also tested using surface electrochemical methods. Three one-electron transfer redox processes in the studied potential range are identified, where only one such a process is associated with the catalyst's ORR activity. The effect of KOH on the Co-N-S/C catalyzed ORR kinetics is investigated using the rotating disk electrode technique in a concentration range of 0.05 to 6.0M. Several ORR kinetic parameters such as overall electron transfer number (n), the product of electron transfer number and coefficient in ORR rate determining step (αn_α), and the exchange current density ($i^o_{O_2/H_2O}$) are estimated. The results show that values of n at different KOH concentrations are close to 4.0, suggesting that Co-N-S/C catalyzed ORR is a 4-electron transfer process from O_2 to H_2O. KOH concentration has an insignificant effect on the value of n, however, a significant effect is observed on both values of αn_α and $i^o_{O_2/H_2O}$. (αn_α decreases while that of $i^o_{O_2/H_2O}$ increases with increasing KOH concentration).

Keywords: Oxygen reduction reaction; Co-Pyridine/C catalyst; KOH concentration effect, alkaline polymer electrolyte membrane fuel cell

1. INTRODUCTION

In the effort to explore clean power sources for automobiles, stationary power stations, and portable power devices, currently, polymer electrolyte membrane (PEM) fuel cells, including both acidic and alkaline electrolyte membranes based PEM fuel cells, have been receiving continued interest due to both their high energy and power densities, high efficiencies and low/zero emissions [1]. However, in the commercialization process, both acidic and alkaline PEM fuel cells face

challenges such as high cost and insufficient durability of key components [2]. One of these challenges resides in reducing the loading of expensive Pt-based catalysts necessary for fuel cell reactions, in particular the cathode oxygen reduction reaction (ORR). These Pt-based catalysts have been identified as the major contributor to the prohibitively high cost of PEM fuel cells. To address this issue, much effort has been made on non-noble metal catalysts and some promising candidates have been developed including transition metal nitrides [3,4] transition metal oxides [5], Co- and Fe-based catalysts [6,7], transition metal macrocycles (porphyrin or phtalocyanine) based catalysts [8-11] as well as other non-precious catalysts [12,13]. Although the ORR activities of such non-noble catalysts are still lower than those of Pt-based catalysts, a continuing incremental improvement in their ORR activities has been seen over the past several decades.

Carbon supported transition metal macrocycle complexes (metal-N_4) such as metalloporphyrins and metallophthalocyanines, either in their as-prepared form or their post heat-treatment form (in an inert atmosphere), have been widely studied as the most promising ORR catalysts in both alkaline and acidic media [14-20]. In particular, when a metal-nitrogen containing material is pyrolyzed at a target high temperature, the molecular structure of the macrocycle in this material will be partially destroyed, forming a catalyst which has a much better ORR catalytic activity and stability than that without pyrolysis. The metal-N_4/N_2 moieties, formed after the pyrolysis, have been identified as the ORR active sites, therefore, the metal ion and the nitrogen related groups in the precursor play important roles in forming such ORR active sites [21]. However, due to the structural complexity of the nitrogen-containing macrocyclic ligands, their high cost is unavoidable. Therefore, using more common, simple, and cost-effective ligands, such as NH_3 and acetonitrile, may be more practical.

With regard to the use of simple nitrogen-containing ligands, recent publications [22-25] are worth mentioning, where nitrogen-containing small molecules, such as ethylene diamine ($NH_2CH_2CH_2NH_2$), together with transition metal salts, such as $Co(NO_3)_2$ and/or $FeSO_4$, were used to prepare active catalysts (carbon supported Co-N_X or Fe-N_X catalysts) for electrochemical reduction of oxygen. In our most recent paper [26], using pyridine as nitrogen-containing ligand and cobalt sulfate heptahydrate ($CoSO_4 \cdot 7H_2O$) as the metal source, we reported the synthesis, structural and electrochemical characterization of carbon-supported Co-pyridine catalysts, and demonstrated their ORR activity in alkaline solution. In addition, the effect of heat-treatment temperature on these catalysts' ORR activities were also studied in alkaline solutions. This is of practical importance because the ORR is more favorable in alkaline electrolytes than in acidic or neutral electrolytes, and consequently, a concentrated alkaline solution, namely, 15-30 wt% KOH (3-7 M), is suitable to ensure sufficient high ionic conductivity that is required for utilizing thick anodes, especially under low-temperature operating conditions [27-29].

As part of a continuing effort, we studied the ORR kinetics catalyzed by heat-treated Co-Pyridine/C (abbreviated as Co-N-S/C) catalysts, and the effect of KOH concentration on both the electrochemical reaction of Co-N-S/C on the electrode surface as well as on the catalyzed ORR kinetics, using surface cyclic voltammetry and rotating disk electrode techniques in 0.05 M to 6.0 M KOH alkaline solutions. It was found that when using an alkaline electrolyte, the Co-N-S/C catalyst showed a significantly enhanced electrocatalytic activity compared to bulk Py/C and Co/C. The catalyzed kinetic parameters, such as ORR overall electron transfer number, the product of electron

transfer number and coefficient in the ORR rate determining step, the exchange current density, and their sensitivities to KOH concentration were also estimated. Based on these results and the literature, a possible mechanism for Co-N-S/C catalyzed ORR was also proposed for facilitating further discussion.

2. EXPERIMENTAL

2.1 Materials and Catalyst synthesis

Co-Pyridine/C catalyst was synthesized from the cobalt-pyridine-carbon precursor, which was prepared from a ground mixture of cobalt sulfate hepathydrate ($CoSO_4{\cdot}7H_2O$, analytically pure), pyridine (Py, analytically pure), Vulcan carbon (Vulcan XC-72R, Carbot) and methanol (analytically pure). After this mixture was dried in vacuum at 40°C for 60 minutes to remove methanol, the resulting powder was divided and then pyrolyzed at 800^{o}C for 2 hours under a nitrogen atmosphere to give the final carbon-supported CoPy catalyst. As reported in our previous paper [26], this heat-treated catalyst is also expressed as Co-N-S/C in this paper.

2.2 Catalyst characterization

As reported in our previous paper [26], the synthesized Co-N-S/C catalysts were physically characterized using crystal-phase X-ray diffraction (XRD), transmission electron microscopy (TEM), energy dispersive X-ray spectroscopy (EDX), field emission scanning electron microscope (FE-SEM), and X-ray photoelectron spectroscopy (XPS), respectively.

2.3 Electrode preparation for electrochemical characterization

For electrochemical cyclic voltammetric (CV) and rotating disk electrode (RDE) experiments, the catalyst sample was coated on a glassy carbon (GC) disk electrode with a geometric surface area of 0.28 cm^2 to form a catalyst layer. For the catalyst coating process, a catalyst ink was prepared by mixing 4 mg catalyst with 2 ml of isopropyl alcohol and sonicated for 15 minutes. Then, 10 μL of such an ink was deposited onto the surface of the GC disk electrode, forming a catalyst layer. After air-drying, 5 μL of a methanol/Nafion® solution (50:1 by mass) was deposited onto the surface of the catalyst and left to dry at room temperature. The overall loading of the catalyst was 7.06×10^{-5} g cm^{-2}, and the Nafion® loading was 3.6×10^{-6} g cm^{-2}.

Both CV and RDE measurements were performed in a standard three-compartment electrochemical cell in KOH solution, ranging in concentration from 0.05 to 6.0 M, at room temperature. A Pt wire and a saturated calomel electrode (SCE) were used as the counter and reference electrodes, respectively, and the catalyst coated GC disk electrode described above was used as the working electrode. All measured potentials in this work were converted into values referring to a standard hydrogen electrode (SHE). An electrochemical instrument system consisting of a potentiostat,

an electrode rotator and a computer (purchased from Pine Instruments), was used for all measurements in this paper. During the measurement, the CVs were first carried out on the freshly prepared working electrode, and the electrolyte solution was deaerated by purging with nitrogen for 30 minutes. The electrode surface was electrochemically cleaned by repeatedly cycling the potential between -0.3 and 0.6 V for more than 30 cycles at a scan rate of 50 mV s^{-1} in the presence of N_2 bubbling. In this case, the electrode surface was determined to be clean when a stable, reproducible voltammogram was recorded. For ORR measurements, the KOH solution was saturated with oxygen (99.999%) under a constant bubbling for 30 minutes before CV or RDE current-voltage curves were collected. For comparison, two other samples, Py/C and Co/C, both of which were heat-treated at 800^{o}C, were also separately used to coat the GC electrodes, and measured using the same procedure as that for the Co-N-S/C coated electrode.

2.4 Oxygen solubility and diffusion coefficient in alkaline solutions containing various KOH concentrations and their viscosities

Table 1. Oxygen solubility and diffusion coefficients in alkaline solutions containing various KOH concentrations and the viscosities of these KOH solutions.

KOH Concentration (M)	C_{O_2} (mol cm^{-3})	D_{O_2} (cm^2 s^{-1})	ν (cm^2 s^{-1})
0.05	1.2×10^{-6}	2.0×10^{-5}	1.0×10^{-2}
0.1	1.1×10^{-6}	1.9×10^{-5}	1.0×10^{-2}
1.0	7.8×10^{-7}	1.8×10^{-5}	1.0×10^{-2}
3.0	3.0×10^{-7}	1.3×10^{-5}	1.2×10^{-2}
6.0	1.7×10^{-7}	7.5×10^{-6}	1.6×10^{-2}
C_{O_2}: O_2 solubility; D_{O_2}: O_2 diffusion coefficient; ν: Viscosity			

For RDE data analysis according to Koutecky-Levich theory, the oxygen solubilities and diffusion coefficients of alkaline solutions containing various KOH concentrations and the viscosities of these KOH solutions are all required. These parameters' values were obtained from the literature [30-32]. The values are summarized in Table 1, which were used to obtain the values of overall electron transfer numbers of the Co-N-S/C catalyzed ORR at different KOH concentrations.

3. RESULTS AND DISCUSSION

3.1 Composition of the Co-N-S/C catalyst

As reported in our previous paper [26], to determine the composition of Co-N-S/C catalysts, EDX analysis was employed to analyze both non-heat-treated and heat-treated catalyst samples. For comparison, a non-pyrolyzed sample, Co-Py/C, was also analyzed.

Table 2. Composition of Co-N-S/C heat-treated at 800°C, measured by EDS

Element in catalyst	Content after heat-treatment (wt%)	Content before heat-treatment (wt%)
C	6.9×10^1	6.0×10^1
Co	2.3×10^1	1.5×10^1
O	5.5×10^0	3.4×10^0
N	1.6×10^0	4.4×10^0
S	1.4×10^o	1.7×10^0

As shown in Table 2, total Co content is measured to be ~23 wt% for the catalyst synthesized at 800°C, which is higher than that for the non-pyrolyzed sample (15 wt% Co in Co^{II}-Py/C). This indicates that pyridine decomposition happened in the Co-Py/C complex during heat-treatment. It can also be seen that the total N content in the heat-treated sample is only 1.6 wt%. If assuming that all of these N atoms are coordinated by Co ions to form ORR active sites, such as Co-N_4, 1.7 wt% of Co will be used. However, the total Co content is 23 wt% as measured by EDX, suggesting that other 21 wt% of Co exist in the forms of metallic Co, Co oxides, and Co-S compounds, which may not be ORR active. Therefore, if assuming the ORR active portion in the Co-N-S/C catalyst is that of Co-N_4, only 1.7 wt% Co in a form of nitrogen-coordinated Co ion is useful in the ORR catalyzed process.

3.2 Surface redox processes of Co-N-S/C catalyst

To understand the electrochemistry of Co-N-S/C catalysts, an electrode coated with this catalyst was tested using CV in alkaline solutions with different KOH concentrations. As an example, Fig. 1 shows the CV curve of Co-N-S/C coated electrodes, recorded in N_2-saturated 6.0 M KOH at a potential scan rate of 25 mV s^{-1}. It can be seen that there are three surface redox waves, marked as Waves I/I', II/II' and III/III', with average peak potentials near -0.107 V, 0.138 V, and 0.501 V vs. SHE, respectively. In addition, the CV curves appear less symmetrical, and the potentials of the anodic and cathodic peaks become slightly separated. This may indicate that surface redox processes have some degree of irreversibility [33].

CVs were also recorded at several potential scan rates, and the peak current densities of the three waves shown in Fig. 1 were also plotted as a function of potential scan rate, as shown in Fig. 2. It can be seen that the peak current densities (I_p) of all three waves show linear relationships with potential scan rate, indicating that their surface behaviors approximately follow that theoretically expected for reversible redox process inside a thin-layer electrode [34].

$$I_p = \frac{Z^2 F^2}{4RT} \Gamma \upsilon \qquad (1)$$

where Z is the electron transfer number involved in the electrochemical reaction, F is the Faraday constant, R is the ideal gas constant, T is the absolute temperature, υ is the potential scan rate, and Γ is the surface concentration of the active species.

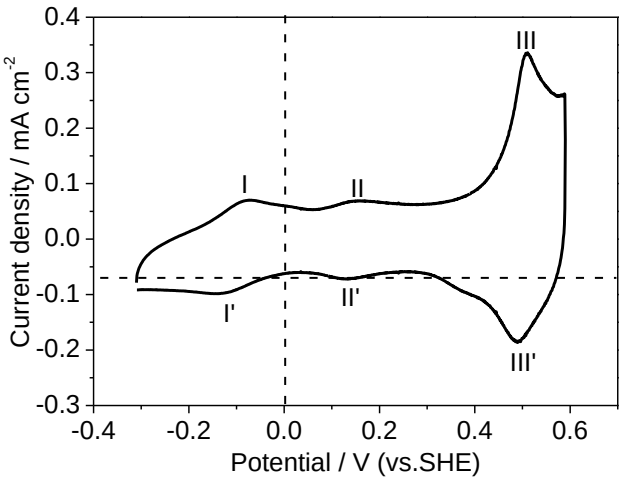

Figure 1. Cyclic voltammogram of Co-N-S/C coated glass carbon disk electrode (0.28 cm^2), recorded in N_2-saturated 6.0 M KOH at a potential scan rate of 25 mV s^{-1}. Catalyst loading: 7.06×10^{-5} g cm^{-2}.

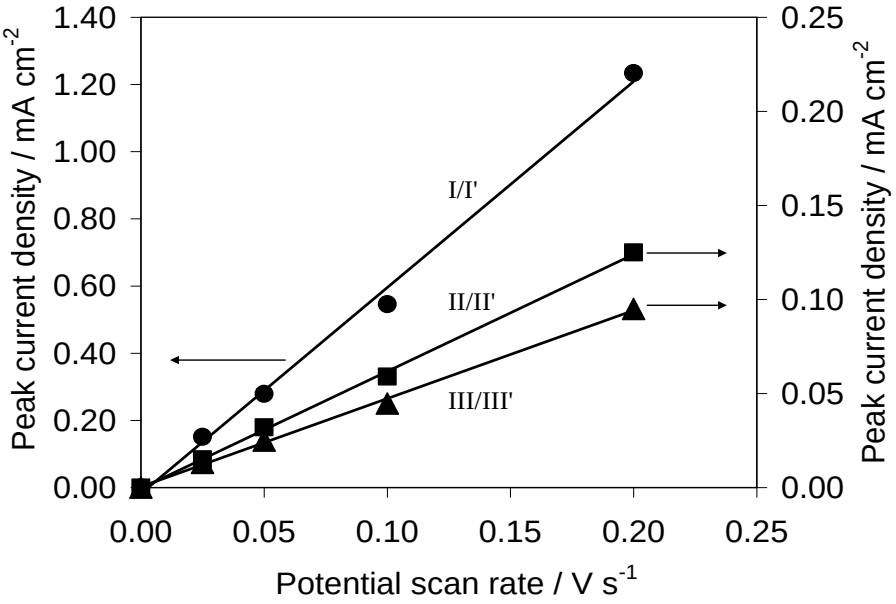

Figure 2. Average peak current densities as a function of potential scan rate. Data recorded under the same conditions as those in Figure 1.

Three $I_p \sim \upsilon$ plots in Fig. 2 yield three slopes ($=\frac{Z^2F^2}{4RT}\Gamma$), from which the surface concentrations of the corresponding redox couples (Γ) can be estimated if Z , F, R, and T are known. In Fig. 1, all three surface waves have an approximate half-peak-width of 80-100 mV, which is close to 90 mV for a one-electron transfer reversible redox process in thin-layer electrode, indicating all of them correspond to a one-electron transfer processes. In case of Z = 1.0, F = 96487 As mol^{-1}, R =

8.314 J mol^{-1} K^{-1}, and T = 298 K, the surface concentrations for Wave I/I', II/II', and III/III', $\Gamma_{I/I'}$, $\Gamma_{II/II'}$, and $\Gamma_{III/III'}$ can be obtained using Equation (1) and the slope values of those three linear plots in Fig. 1, are 6.62×10^{-10}, 4.99×10^{-10}, and 6.72×10^{-9} mol cm^{-2}, respectively. If all of these three waves come from the redox processes at the Co center, the total Co surface concentration (Γ_{Co}) would be the sum of these three surface concentrations:

$$\Gamma_{Co} = \Gamma_{I/I'} + \Gamma_{II/II'} + \Gamma_{III/III'} \quad (2)$$

The calculated result according to Equation (2) is then 7.88×10^{-9} mol cm^{-2}.

3.3 Effect of OH^- concentration on Co-N-S/C catalyst redox processes

In order to investigate the effect of OH^- concentration on the redox processes expressed by Waves I/I', II/II' and III/III', the surface CVs were also recorded in solutions each in different KOH concentrations such as 0.05, 0.1, 1.0, 3.0, and 6.0 M, respectively. It was observed that both the average peak potentials of Wave II/II' and Wave III/III' were shifted in the negative direction with increasing KOH concentration, however the average peak potential of Wave I/I' shifted very little with increasing KOH concentration. For a more quantitative analysis, the average peak potentials of these three waves are plotted as a function of log($[OH]^-$), as shown in Fig. 3. For these three redxox waves, the linear plots of average peak potential vs. log($[OH]^-$) yield three slopes, which are -0.069, -0.127, and -0.126 V $(\log([OH]^-))^{-1}$ for Waves I/I', II/II' and III/III', respectively.

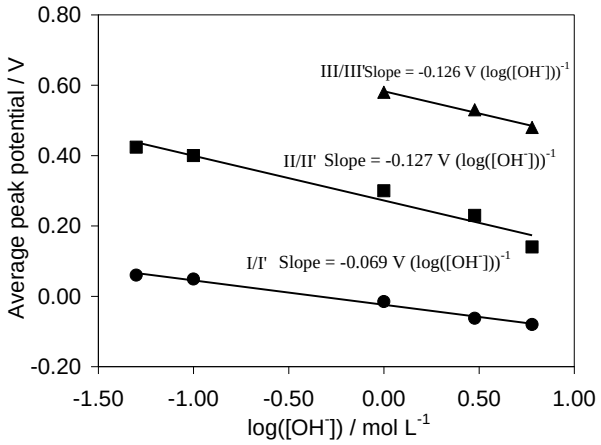

Figure 3. Average peak potentials as a function of log ($[OH^-]$) for Wave I/I', II/II', and III/III' shown on Fig. 1. (Experimental conditions are the same as those in Fig. 1)

For a reversible redox process with an electron transfer number of Z and OH^- ion number of m: $O + Ze^- \leftrightarrow R + mOH^-$, where O is the oxidant, and R is the reductant, the Nernst equation can be used to describe the relationship between the electrode potential ($E_{O/R}$) and the concentrations of O and R:

$$E_{O/R} = E^o_{O/R} + \frac{0.0592}{Z}\log(\frac{[O]}{[R][OH^-]^m})$$
$$= E^o_{O/R} - 0.0592\frac{m}{Z}\log(\frac{[O]}{[R]}[OH^-]) \quad (3)$$
$$= E^o_{O/R} - 0.0592\frac{m}{Z}\log(\frac{[O]}{[R]}) - 0.0592\frac{m}{Z}\log([OH^-])$$

where $E_{O/R}$ is the standard electrode potential of the redox reaction, [*O*] and [*R*] are the molar concentrations of oxidant and reductant, respectively. According to this equation, the slope of the plot of $E_{O/R}$ *vs.* $\log([OH^-])$ is $-0.0592\frac{m}{Z}$. If Z is known, *m* can be calculated using this slope expression, which indicates how many OH^- ions are involved in the redox process.

For Wave I/I', which is a one-electron redox process, the plot slope of average peak potential *vs*. log([OH^-]) ($=-0.0592\frac{m}{1}$)is -0.069 Vlog([OH^-]), meaning that *m* is very close to 1, suggesting that the redox process of Wave I/I' is a one-electron transfer and one OH^- is involved in the process. In the similar way, using the slope values obtained by Fig. 3, one can obtain the redox processes of Waves II/II' and III/III', which are both one-electron transfer and two-OH^- involved processes, respectively. According to the numbers obtained for electron transfer and OH^- ions in each redox process, the possible assignments to these three waves may be proposed, respectively:

$$K[(OH^-)Co(III)NS]/C + e^- \leftrightarrow K[Co(II)NS]/C + OH^- \quad \text{(Wave I/I')} \quad \text{(I)}$$

$$KCo(III)(OH)_4/C + e^- \leftrightarrow Co(II)(OH)_2/C + 2OH^- + K^+ \quad \text{(Wave II/II')} \quad \text{(II)}$$

$$K_2Co(IV)(OH)_6/C + e^- \leftrightarrow KCo(III)(OH)_4/C + 2OH^- + K^+ \quad \text{(Wave III/III')} \quad \text{(III)}$$

Among these three waves, only Wave I/I' corresponds to the portion containing nitrogen, therefore, it may be the only ORR active portion in the entire catalyst. According to the surface concentrations of these three waves, as discussed in Fig. 1, the percentage of this nitrogen containing portion in the total Co related composition should be:

$$\frac{\Gamma_{I/I'}}{\Gamma_{Co}}\% = \frac{\Gamma_{I/I'}}{\Gamma_{I/I'} + \Gamma_{II/II'} + \Gamma_{III/III'}} \times 100$$
$$= \frac{6.62X10^{-10}}{6.62\times10^{-10} + 4.99X10^{-10} + 6.72\times10^{-9}} \quad (4)$$
$$= 8.40\%$$

According to the discussion for Table 2, assuming all of the 1.6 wt% N atoms in the catalyst are coordinated by Co ions to form Co-N_4, 1.7 wt% of Co will be used. The ratio of this 1.7 wt% to the total Co content of 23 wt% will be 7.40%, which is very close to the ratio value of 8.40% for N-coordinated Co obtained by Equation (4), indicating that the EDX measured portion of N-coordinated

Co in the entire catalyst is in an agreement with that measured by surface cyclic voltammtery. This agreement gives a support to the assignment of Wave I/I' to the $K[(OH^-)Co(III)NS]/C \leftrightarrow K[Co(II)NS]/C$ redox couple. In a later section, we will see only Wave I/I' is ORR active, while the other two (Waves II/II' and III/III') are ORR inactive. This may be because the corresponding redox couples of the two waves do not contain any nitrogen groups.

3.4 ORR activities of Waves I/I', II/II' and III/III'

To test the catalytic activity of the prepared Co-N-S/C catalyst for the ORR, the catalyst coated electrode was also measured in O_2-saturated solutions. As an example, Fig. 4 shows a cyclic voltammogram recorded on an electrode coated with Co-N-S/C catalyst in an O_2-saturated 0.1M KOH solution.

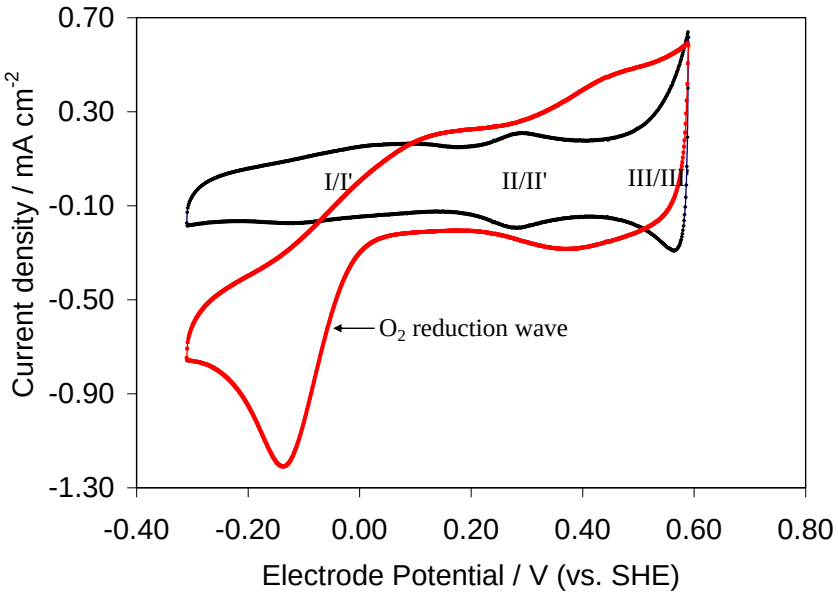

Figure 4. Cyclic voltammograms recorded on a glassy carbon (GC) disk electrode (0.28 cm^2) coated with Co-N-S/C catalyst in N_2-saturated and O_2-saturated 0.1M KOH solutions, respectively. The catalyst was obtained by heat-treating Co(II)-Pyridine/C precursor at 800°C. Potential scan rate: 25 mV s^{-1}, and catalyst loading: 7.06×10^{-5} g cm^{-2}.

For comparison, the same electrode was also tested in a O_2-saturated 0.1M KOH solution, and the CV obtained is also plotted in Fig. 4. It can be seen that in the presence of O_2, a large reduction wave appears with an onset potential close to that of surface Wave I/I', suggesting that the surface redox process expressed by Wave I/I' is responsible for ORR catalytic activity. As shown in Reaction (I), the redox couple is $K[(OH^-)Co(III)NS]/C \leftrightarrow K[Co(II)NS]/C$, indicating that $K[Co(II)NS]/C$ should be responsible for the ORR activity. Fig. 4 also shows that there is no significant ORR current near both Waves II/II' and III/III', probably suggesting that these two waves are not ORR active. A more detailed discussion of the Co-N-S/C catalyzed ORR mechanism will be given in a later section of this paper.

3.5 Rotating disk electrode studies of O_2 reduction reaction

For testing the effect of KOH concentration on Co-N-S/C catalyzed ORR kinetics, the current-voltage (I-V) curves for the Co-N-S/C coated electrode were recorded using a RDE in O_2-saturated solutions containing various KOH concentrations. As an example, Fig. 5 shows three typical I-V curves for 0.1, 1.0 and 3.0 M KOH, respectively, at an electrode rotation rate of 1500 rpm. It can be seen that the ORR current density increases with decreasing electrode potential, and when the potential is negative enough, a plateau current density is reached, suggesting that current density reaches a limitation in O_2 diffusion from the solution to the electrode surface. Actually, the current densities in the entire potential range, as shown in Fig. 5, are composed of two portions which are, the ORR kinetic current density, and the O_2 diffusion current density.

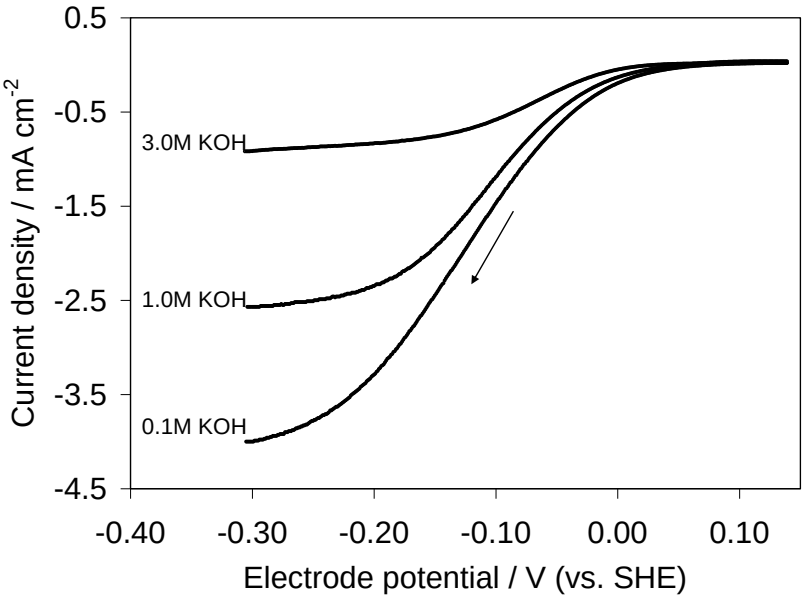

Figure 5. Current-voltage curves recorded using a GC disk electrode (0.28 cm^2) coated by Co-N-S/C catalyst in O_2-saturated alkaline solutions with three different KOH concentrations as marked. The electrode potential scan rate: 5 mV s^{-1}; electrode rotating rate: 1500 rpm; catalyst loading: 7.06×10^{-5} g cm^{-2}.

At a relatively positive potential range (for example, more positive than -0.05V vs. SHE in Fig. 5, the current density is dominated by the ORR kinetic process, and at a relative negative potential range (more negative than -0.10 V vs. SHE), the current density is mainly limited by O_2 diffusion process. The I-V curves shown in Fig. 5 indicate that when increasing the KOH concentration, the current densities increase in the entire studied potential range. This reduction in current density is mainly caused by the reductions in O_2 solubility and the O_2 diffusion coefficient, as well as the increase in KOH solution viscosity, as shown in Table 1, when the KOH concentration is increased. According to RDE theory (also called Koutecky-Levich theory), the disk current density (i_d, A cm^{-2}),

as shown in Fig. 5, can be expressed as the combination of two current densities, the ORR kinetic current density (i_k, A cm^{-2}) and the O_2 diffusion related current density (i_L, A cm^{-2}):

$$i_d = \left(\frac{1}{i_k} + \frac{1}{i_L} \right)^{-1} \quad (5)$$

Because the electrode catalyst layer contains an ionomer, the O_2 diffusion related limiting current density (i_L) should contain a contribution from O_2 diffusion through the ionomer layer (i_f) [35]. Therefore i_L can be expressed as: $i_L = \left(\frac{1}{i_l} + \frac{1}{i_f} \right)^{-1}$ where i_l is the limiting current density induced by O_2 diffusion from solution through catalyst layer. Then, Equation (5) becomes Equation (6) [36]:

$$i_d = \left(\frac{1}{i_k} + \frac{1}{i_l} + \frac{1}{i_f} \right)^{-1} \quad (6)$$

In Equation (6), three current densities (i_k, i_l, and i_f) are all related to O_2 concentration:

$$i_k = nFk\Gamma_{I/I'}C_{O_2} \exp\left(-\frac{\alpha n_\alpha F(E-E^o)}{RT} \right) = i^o_{O_2/H_2O} \exp\left(-\frac{\alpha n_\alpha F(E-E^o)}{RT} \right) \quad (7)$$

$$i_l = 0.201nFC_{O_2}D_{O_2}^{2/3}\nu^{-1/6}\omega^{1/2} \quad (8)$$

$$i_f = \frac{nFC^f_{O_2}D^f_{O_2}}{L} \quad (9)$$

For Equation (7), the reaction order for O_2 concentration is treated as the first order. Where n is the ORR overall electron transfer number, F is Faraday's constant (96487 C mol^{-1} or A s mol^{-1}), k is the standard reaction constant of ORR (mol^{-1} cm^3 s^{-1}), $\Gamma_{I/I'}$ is the surface concentration of Co-N-S/C defined by Wave I/I' in Fig. 1 (mol cm^{-2}), C_{O_2} is the concentration (or solubility) of O_2 in the electrolyte solution (mol cm^{-3}), $i^o_{O_2/H_2O}$ is defined as the exchange current density of the catalyzed ORR (mol cm^{-2}), which can be expressed as $i^o_{O_2/H_2O} = nFk\Gamma_{I/I'}C_{O_2}$, α is the electron transfer coefficient in the ORR rate determining step, n_α is the electron transfer number in the ORR rate determining step, E is the electrode potential (V *vs*. SHE), E^o is the thermodynamic ORR electrode potential (V *vs*. SHE), which can be expressed as $E^o = -0.828 - 0.0592\log([OH^-]$ at 25^{o}C and 1.0 atm O_2 atmosphere, R is the ideal gas constant (8.314 J mol^{-1} K^{-1}), and T is the absolute temperature (K). It can be seen that this kinetic current density is a function of electrode potential. Its magnitude increases exponentially when the potential further shifts in the negative (cathodic) direction. For Equation (8), D_{O_2} is the diffusion

coefficient of O_2 (cm^2 s^{-1}), ν is the viscosity of the KOH aqueous solution (cm^2 s^{-1}), and ω is the electrode rotating rate (rpm). In this equation, any reduction in value of C_{O_2} or D_{O_2}, or any increase in ν can cause a decrease in the diffusion limited current density. For Equation (9), $C_{O_2}^f$ and $D_{O_2}^f$ are the solubility and diffusion coefficients of O_2 in the ionomer of catalyst layer, and L is its equivalent thickness, which can be estimated according to $L = 0.1\frac{X_{nf}V_s\rho_s}{\rho_{nf}A_{gc}}$ (where X_{nf} is the mass fraction of ionomer in the ionomer solution, V_s is the volume of the deposited aliquot, ρ_s is the density of ionomer solution, ρ_{nf} is the ionomer density, and A_{gc} is the GC electrode surface area. According to this L expression, the thickness of the Nafion® ionomer layer in our experiment was calculated to be 1.8×10^{-6} cm, assuming that the density of Nafion® film is 2.0 g cm^{-3} [37]. According to Equation (9), the O_2 diffusion current density through the equivalent Nafion® ionomer film in the catalyst layer was calculated to be 1.98 A cm^{-2} if the values of $C_{O_2}^f$ and $D_{O_2}^f$ were adopted as 1.56×10^{-5} mol cm^{-3}, and 6.16×10^{-7} cm^2 s^{-1}, respectively [38]. Note that for this calculation, the values of n and F were taken as 4.0 and 96487 A s mol^{-1}, respectively. This current density is much higher than those current densities collected in our RDE experiments. Therefore, its' reciprocal can be negligible when compared to those of both those of i_k and i_l. In this case, Equation (6) can be simplified to:

$$\frac{1}{i_d} = \frac{1}{i_k} + \frac{1}{i_l} = \frac{1}{i_{O_2/H_2O}^o \exp\left(-\frac{\alpha n_\alpha (E - E^o)}{RT}\right)} + \frac{1}{0.201nFC_{O_2}D_{O_2}^{2/3}\nu^{-1/6}}\omega^{-1/2} \quad (10)$$

From Equation (10), it can be seen that a change in O_2 concentration can result in a proportional change to the magnitudes of both kinetic and diffusion current densities. The concentration of KOH in the electrolyte affects the saturated O_2 concentration. It follows that different solutions containing different concentrations of KOH will result in different O_2 concentrations, which in turn lead to changes in these two aforementioned current densities. We will give a detailed discussion about these changes induced by KOH concentration in the following sections.

3.5.1. ORR kinetic parameters estimated using RDE data at different electrode rates and Koutecky-Levick theory

In order to investigate the effect of O_2 concentration on the catalyzed ORR, the I-V curves were further recorded at different electrode rotating rates. Fig. 6 shows the I-V curves recorded at electrode rotation rates from 300 to 2400 rpm in O_2-saturated 3.0 M KOH solution. It can be seen that the current density at the diffusion dominated potential range increases with increasing electrode rotation rate, which can be expected from Equation (10).

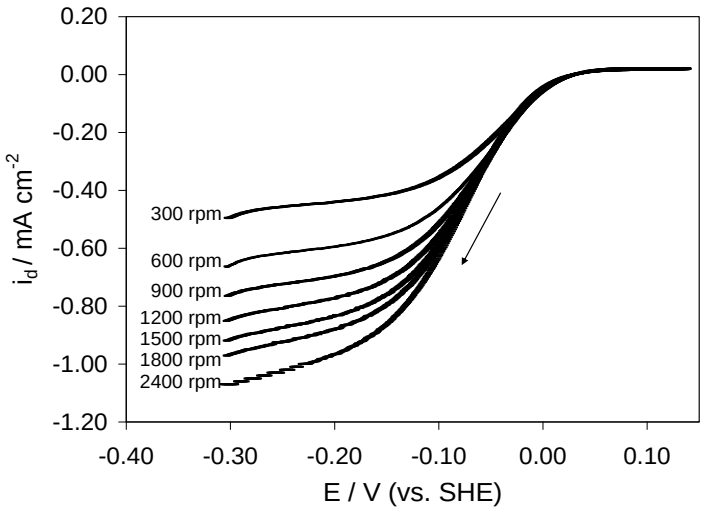

Figure 6. Current-voltage curves recorded on the Co-N-S/C catalyst coated GC disk electrode (0.28 cm^2) at different electrode rotation rates as marked in O_2-saturated 3.0M KOH solution. Other conditions are the same as those in Fig. 5.

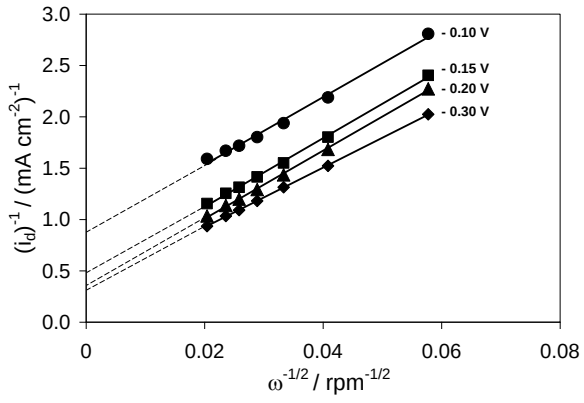

A

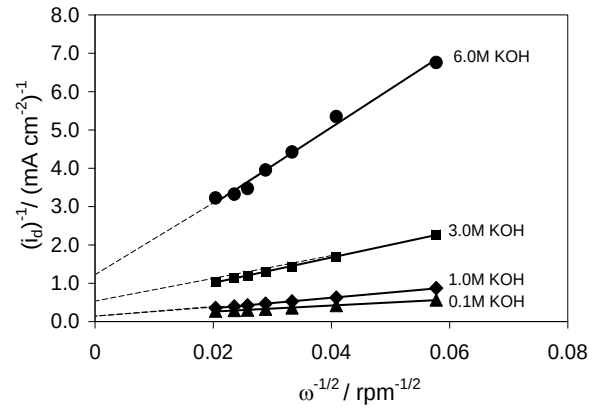

B

Figure 7. (a) Koutecky-Levich plots at different electrode potentials (data from Fig. 6); (b) Koutecky-Levich plots at different KOH concentrations (data recorded at the same conditions as those in Fig. 5).

According to Equation (10), the I-V data at different electrode potentials were plotted in order to obtain the kinetic current densities. As an example, Fig. 7(a) shows the plots at four typical electrode potentials such as -0.10, -0.15, -0.20, and -0.30 V vs. SHE, and Fig. 7(b) shows the plots at four typical KOH concentrations such as 0.1, 1.0, 3.0, and 6.0M, respectively.

3.5.2. Effect of KOH concentration on ORR kinetic parameters

According to Equation (10), the slope of the plot shown in Fig. 7 can be used to estimate the overall electron number for the Co-N-S/C catalyzed ORR, which can be expressed as the inverse of $0.201nFC_{O_2}D_{O_2}^{2/3}\gamma^{-1/6}$. If the values of F, C_{O_2}, D_{O_2}, and ν are known, the value of n can then be calculated according to the obtained slope value. At electrode potentials of -0.10, -0.15, -0.20, and -0.30 V vs. SHE, the obtained overall ORR electron transfer numbers at each of these potential are close with some slight variation. Table 3 shows the average ORR overall electron transfer numbers at different KOH concentrations.

Table 3. Average ORR electron transfer numbers catalyzed by Co-N-S/C catalyst at different KOH concentrations.

KOH concentration (M)	0.05	0.10	1.0	3.0	6.0
Average ORR overall electron transfer number (*n*)	4.00	3.84	3.52	3.80	3.58

It can be seen that all values are closed to 4, indicating that the Co-N-S/C catalyst can catalyze the 4-electron ORR reaction producing water. Some numbers are less than 4 suggesting that the catalyzed ORR mechanism is probably a 2+2 electron transfer pathway, that is, the first 2-electron transfer pathway produces peroxide, and the second is the further reduction of this peroxide to water. It can also be seen that, with increasing KOH concentration, the overall electron transfer numbers are decrease slightly, suggesting that at a higher KOH concentration, the first 2-electron transfer pathway from O_2 to peroxide becomes favored or that of the second 2-electron transfer pathway is depressed. This can also be qualitatively explained by the following proposed ORR mechanism based on the authors' understanding [26]:

$$[[Co(II)NS]/C]^{-} + O_2 \leftrightarrow [[O_2 - Co(II)NS]/C]^{-} \quad \text{(IV)}$$

$$[[O_2 - Co(II)NS]/C]^{-} + e^{-} \rightarrow [[O_2^{-} - Co(II)NS]/C]^{2-} \text{ (Rate-determining step)} \quad \text{(V)}$$

$$[[O_2^{-} - Co(II)NS]/C]^{2-} + e^{-} + H_2O \rightarrow [[HO_2^{-} - Co(II)NS]/C]^{2-} + OH^{-} \quad \text{(VI)}$$

$$[[HO_2^{-} - Co(II)NS]/C]^{2-} + 2e^{-} + H_2O \rightarrow [[Co(II)NS]/C]^{-} + 3OH^{-} \quad \text{(VII)}$$

Here, Reaction (IV) is the oxygen adsorption step to form an adduct, Reaction (V) is the first electron transfer step, which may be considered the rate-determining step, Reaction (VI) represents HO_2^- formation, and Reaction (VII) is a 2-electron transfer process to produce the final product (OH^-). Note that this mechanism may or may not represent the true mechanism. We propose it with the goal of facilitating further discussion. From Reaction (VII), it can be seen that with increasing KOH concentration, this reaction will become more difficult, likely leading to a decrease in the overall ORR electron transfer number to less than 4. This is in agreement with the data trend shown in Table 3 for ORR electron transfer data with increasing KOH concentration.

In Fig. 7, the intercept at Y-axis is the value of $\frac{1}{i_k}$, which is equal to $\frac{1}{i^o_{O_2/H_2O}\exp\left(-\frac{\alpha n_\alpha F(E-E^o)}{RT}\right)}$, and can be expressed as: $\frac{1}{i_k}=\frac{1}{i^o_{O_2/H_2O}\exp\left(-\frac{\alpha n_\alpha F(E-E^o)}{RT}\right)}$. Rearranging this expression, Equation (11) can be obtained:

$$E=\frac{RT}{\alpha n_\alpha F}\ln(i^o_{O_2/H_2O})+E^o-\frac{RT}{\alpha n_\alpha F}\ln(i_k) \qquad (11)$$

Equation (11) is the Tafel form. Using the data obtained from those plots, similar to those in Fig. 7, according to Equation (11), the plots of E vs. $\ln(i_k)$ at different KOH concentrations can be made, which can give both intercepts and slopes, from which the ORR exchange current densities ($i^o_{O_2/H_2O}$) and the products of ORR electron transfer number and coefficient (αn_α) can be calculated, respectively.

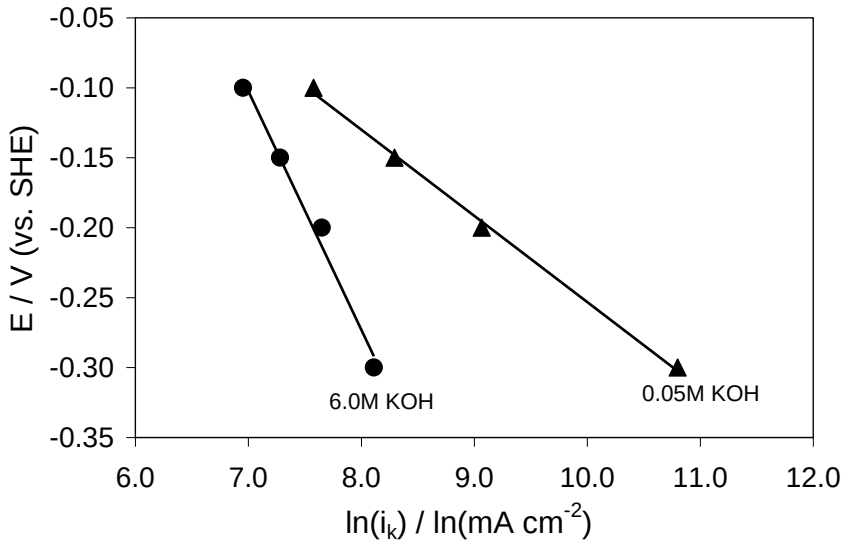

Figure 8. Tafel plots at two different KOH concentrations. The data recorded at the same conditions as those in Fig. 5.

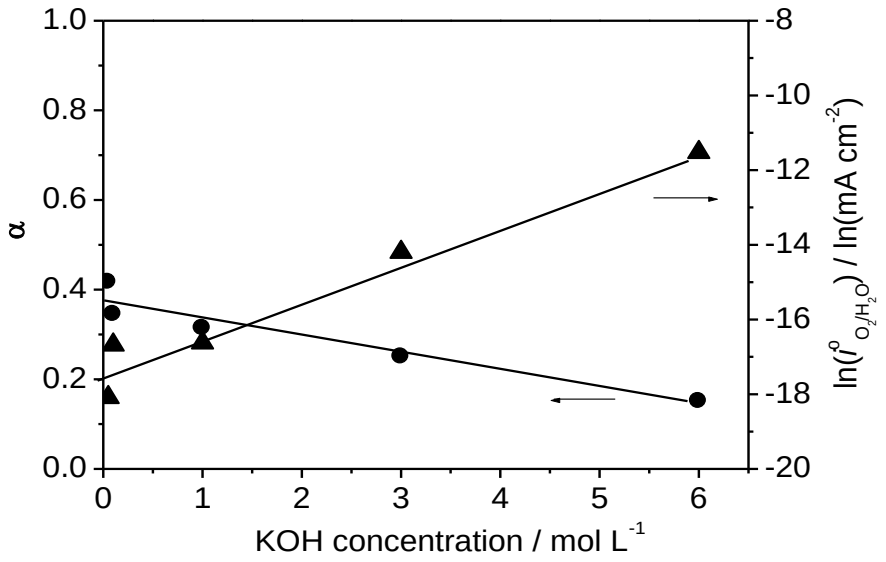

Figure 9. ORR exchange current density and electron transfer coefficient in the rate determining step as a function of KOH concentration. Data from Table 4.

Table 4. Co-N-S/C catalyzed ORR thermodynamic and kinetic parameters in O_2-saturated solutions with different KOH concentrations

KOH concentration (M)	Standard electrode potential of O_2/H_2O at 25°C (E^o, V vs. SHE)	Product of ORR electron transfer number and coefficient (αn_α)	ORR exchange current density ($i^o_{O_2/H_2O}$, A cm^{-2})
0.05	-0.751	0.417	1.40×10^{-8}
0.10	-0.769	0.345	5.71×10^{-8}
1.0	-0.828	0.314	6.03×10^{-8}
3.0	-0.856	0.250	6.83×10^{-7}
6.0	-0.874	0.151	9.89×10^{-6}

As an example, Fig. 8 shows two typical plots at 0.05 and 6.0M KOH, respectively. The parameters obtained at different KOH concentrations are listed in Table 4. For a more clear presentation, Fig. 9 shows the plots of both $\ln(i^o_{O_2/H_2O})$ and α (assuming $n_\alpha = 1$) as a function of KOH concentration. It can be seen that the product of ORR electron transfer number and coefficient (αn_α) decreases with increasing KOH concentration. If the electron transfer number in the ORR rate determining step is assumed to be 1.0 ($n = 1$), the numbers of αn_α shown in Table 4 represent the electron transfer coefficients of the Co-N-S/C catalyzed ORR.

Table 4 and Fig. 9 also show that the ORR exchange current density monotonically increases with increasing KOH concentration. This result indicates that an increase in KOH concentration can positively affect the Co-N-S/C catalyzed ORR kinetics.

According to Equation (7), the ORR exchange current density ($i^o_{O_2/H_2O}$) in Equation (11) can be expressed as Equation (12):

$$i^o_{O_2/H_2O} = nFk\Gamma_{I/I'}C_{O_2} = nFk_o^{1-\alpha}\Gamma_{I/I'}C_{O_2} \quad (12)$$

Where we assume that k could be related to the electron transfer coefficient by $k = k_o^{1-\alpha}$ where k_o is a constant independent of α. Table 4 shows that this α decreases with increasing KOH concentration, suggesting that k is indeed a function of KOH concentration. C_{O_2} in Equation (12) can be expressed as a function of KOH concentration (C_{OH^-}) according to the data listed in Refs [30-32]: $C_{O_2} = e^{0.041543C^2_{OH^-} - 0.58044C_{OH^-} - 6.7011}$ (only applicable for a KOH concentration range of 0.05 - 6M). Then Equation (12) can be rewritten as:

$$i^o_{O_2/H_2O} = nFk_o^{1-\alpha}\Gamma_{I/I'}e^{0.041543C^2_{OH^-} - 0.58044C_{OH^-} - 6.7011} \quad (13)$$

Or $\ln(i^o_{O_2/H_2O}) = \ln(nF\Gamma_{I/I'}) + (1-\alpha)\ln k_o + 4.15X10^{-2}C^2_{OH^-} - 5.80X10^{-1}C_{OH^-} - 6.70X10^0$ (13a)

From Fig. 9, α can be related to KOH concentration with the empirical expression:

$$\alpha = -0.03829C_{OH^-} + 0.3731 \quad (14)$$

Substituting Equation (14) into Equation (13a), Equation (15) can be obtained:

$$\ln(i^o_{O_2/H_2O}) = \ln(nF\Gamma_{I/I'}) + (3.83X10^{-2}C_{OH^-} + 6.27X10^{-1})\ln k_o + 4.15X10^{-2}C^2_{OH^-} - 5.80X10^{-1}C_{OH^-} - 6.70X10^0 \quad (15)$$

Using the plot shown in Fig. 9, the relationship between $\ln(i^o_{O_2/H_2O})$ and KOH concentration (C_{OH^-}) can also be formulated into an equation:

$$\ln(i^o_{O_2/H_2O}) = 1.01X10^0 C_{OH^-} - 1.75X10^1 \quad (16)$$

Combining Equation (16) with Equation (15), the expression of k_o can be obtained:

$$\ln(k_o) = \frac{-\ln(nF\Gamma_{I/I'}) - 4.15X10^{-2}C^2_{OH^-} + 1.58X10^0 C_{OH^-} + 2.42X10^1}{3.83X10^{-2}C_{OH^-} + 6.27X10^{-1}} \quad (17)$$

Using Equation (17), if n, F, $\Gamma_{I/I'}$ and C_{OH^-} are known, k_o can be obtained. Note that Equations (13)-(17) are only applicable at room temperature, ambient pressure and in the KOH concentration range of 0.05 to 6.0 M, and the treatment is semi-empirical.

For this positive effect of KOH concentration on the exchange current density (shown in Table 4 and Fig. 9), the rate-determining step (Reaction (V)) may be used to give an insight into this effect. Normally, the O_2^- ion is more stable in a more concentrated OH^- solution, implying that $[[O_2^- - Co(II)NS]/C]^{2-}$ in Reaction (V) may be more stable. A more stable $[[O_2^- - Co(II)NS]/C]^{2-}$ suggests that by increasing the KOH concentration, Reaction (V) would become faster and easier, probably leading to a higher ORR exchange current density.

4. CONCLUSIONS

Using a simple thermal method, non-noble metal electrocatalysts (Co-N-S/C) were successfully synthesized. The composition of Co-N-S/C was analyzed using EDS, and found that only 1.7 wt% Co is useful in the catalyzed ORR process as a form of nitrogen-coordinated Co ion. The electrochemical activity of such a catalyst was also tested using surface electrochemical methods. Surface cyclic voltammograms of this catalyst revealed that there were three one-electron transfer redox processes in the potential range studied. These three redox processes were studied in solutions containing different KOH concentrations. The KOH concentration dependences of these three waves' average peak potentials were obtained, which were used to propose their surface electrochemical reactions. Regarding the ORR activity catalyzed by the surface redox process, among three redox processes only the process of $K[(OH^-)Co(III)NS]/C + e^- \leftrightarrow K[Co(II)NS]/C + OH^-$ was identified as the ORR active reaction, in which $K[Co(II)NS]/C$ might participate in the ORR process.

The effect of KOH on the Co-N-S/C catalyzed ORR kinetics was investigated using rotating disk electrode technique in a concentration range of 0.05 to 6.0M. several ORR kinetic parameters such as overall electron transfer number (n), the product of electron transfer number and coefficient in the ORR rate determining step (αn_α), and the exchange current density ($i^o_{O_2/H_2O}$) were estimated. The results showed that the ORR overall electron transfer numbers at different KOH concentrations were all close to 4.0, suggesting that Co-N-S/C catalyzed ORR was a 4-electron transfer process from O_2 to H_2O, and that KOH concentration had an insignificant effect on the overall electron transfer number. However, both αn_α and $i^o_{O_2/H_2O}$ were significantly affected by the change of KOH concentration. αn_α decreased with increasing KOH concentration, while $i^o_{O_2/H_2O}$ monotonically increased with increasing KOH concentration, suggesting that increasing KOH concentration could benefit the catalyzed ORR process.

ACKNOWLEDGMENTS

This work was supported by the National Natural Science Foundation of China (21173039); Specialized Research Fund for the Doctoral Program of Higher Education, SRFD (20110075110001) of China, the State Environmental Protection Engineering Center for Pollution Treatment and Control

in Textile Industry of China and the Shanghai Leading Academic Discipline Project (B604) Fund. All the financial supports are gratefully acknowledged.

References

1. M. P. Hogarth, T. R. Ralph, *Platinum Met. Rev*. 46 (2002) 146.
2. T. R. Ralph, M. P. Hogwarth, *Platinum Met. Rev*. 46 (2002) 3.
3. C. Medard, M. Lefevre, J. P. Dodelet, G. Lindbergh, *Electrochim. Acta* 51 (2006) 3202.
4. H. X. Zhong, H. M. Zhang, J. W. Hu, B.L. Yi, *Electrochem. Commun*. 8 (2006) 707.
5. J. H. Kim, A. Ishihara, S. Mitsushima, N. Kamiya, K. I. Ota, *Electrochim. Acta* 52 (2007) 2492.
6. C. W. B. Bezerra, L. Zhang, K. Lee, H. Liu, H. J. Wang, J. J. Zhang, *Electrochim. Acta* 53 (2008) 4937.
7. F. Charreteur, S. Ruggeri, F. Jaouen, J. P. Dodelet, *Electrochim. Acta* 9 (2008) 1.
8. G.. Lalande, G.. Faubert, R. Côté, D. Guay, J. P. Dodelet, L. T. Weng, *J. Power Sources* 61 (1996) 227.
9. J. H. Zagal, S. Griveau, K. I. Ozoemena, T. Nyokong, F. Bedioui, *J Nanosci Nanotechnol*, 9 (2009) 2201.
10. Z. Xu, H. Li, G. Cao, Q. Zhang, K. Li, X. Zhao, *J. Mol. Catal. A Chem*. 335 (2011) 89.
11. H. Liu, C. Song, Y. Tang, J. Zhang, *Electrochim. Acta* 52 (2007) 4532.
12. C. W. B. Bezerra, L. Zhang, K. Lee, H. Liu, A. L .B. Marques, E. P. Marques, H. Wang, J. Zhang, *Electrochim. Acta* 53 (2008) 4973.
13. A. Serov, M. H. Robson, B. Halevi, K. Artyushkova, P. Atanassov, *Electrochem. Commun*. 22 (2012) 53.
14. Z.P. Li, B.H. Liu, *J. Appl. Electrochem*. 40 (2010) 475.
15. E. Hao Yu, S. Cheng, B.F. Logan, K. J. Scott, *J. Appl. Electrochem*. 39 (2009) 705.
16. R. R. Chen, H. X. Li, D. Chu, G. F. Wang, *J. Phys. Chem*. C 113 (2009) 20689.
17. Y. Lu, R.G. Reddy, *Int. J. Hydrogen Energy* 33 (2008) 3930.
18. H. Schulenburg, S. Stankov, V. Schunemann, J. Radnik, I. Dourbandt, S. Fiechter, P. Bogdanoff, H. Tributsch, *J. Phys. Chem*. B 107 (2003) 9034.
19. M. Ladouceur, G. Lalande, D. Guay, J.P. Dodelet, *J. Electrochem. Soc*. 140 (1993) 1974.
20. V. Bambagioni, C. Bianchini, J. Filippi, A. Lavacchi, W. Oberhauser, A. Marchionni, S. Moneti, F. Vizza, R. Psaro, V. D. Santo, A. Gallo, S. Recchia, L. Sordelli, *J. Power Sources* 196 (2011) 2519.
21. M. Lefèvre, J. P. Dodelet, P. Bertrand. *J. Phys. Chem*. B, 104 (2000) 11238.
22. X. G. Li, B. N. Popov, T. Kawahara, H. Yanagi, *J. Power Sources* 196 (2011)196, 1717.
23. G. Liu, X. G. Li, P. Ganesan, B. N. Popov, *Electrochim. Acta* 55 (2010) 2853.
24. Li, X.G., Liu, G., Popov, B. N.. *J. Power Sources* 195 (2010) 6373.
25. G. Liu, X. G. Li, P. Ganesan, *Appl. Catal. B: Environ*. 93 (2009) 156.
26. J. L. Qiao, L. Xu, L. Dinga, L. Zhang, R. Baker, X. F. Daia, J. J. Zhang, *Applied Catalysis B: Environ.* 125 (2012) 197.
27. H. Arai, M. Hayashi, Secondary batteries: metal-air systems. In: Garche J, editor. Incyclopaedia of electrochemical power sources. 2010: pp347- 355.
28. O. Haas, J. V. Wesemael, Zinc-air: electrical recharge. In:Garche J, editor. Incyclopaedia of electrochemical power sources. 2010: pp384-92.
29. K. Kinoshita, Electrochemical oxygen technology. New York: John Wiley & Sons Inc; 1992.
30. R. E. Davis, G. L. Horvath, C. W. Tobias, *Electrochim. Acta*, 12 (1967) 287
31. K. E. Gubbins, R. D. Walker, Jr. *J. Electrochem. Soc*. 112 (1965) 469
32. CRC Handbook of Chemistry and Physics, Edition 92 (2007)
33. J. F. Ni, H.H. Zhou, J.T. Chen, X.X. Zhang, *Mater. Lett*. 59 (2005) 2361.

34. A. J. Bard, L. R. Faulkner, Electrochemical Methods, Fundamentals and Applications, Wiley, New York, 1980.
35. W. Vielstich, A. Lamm, H.A. Gasteiger, Handbook of Fuel Cells-Fundamentals, Technology and Applications: Rotating thin film method for supported catalysis, John Wiley&Sons, New York, 2003, Chap. 22, pp. 316-333.
36. T.J. Schmidt, H.A. Gasteiger, in: W. Vielstich, A. Lamm, H.A. Gasteiger (Eds.), Handbook of Fuel Cells-Fundamentals, Technology and Applications: Rotating Thin Film Method for Supported Catalysis, John Wiley & Sons, New York, 2003, p. 316, Chap. 22
37. O. A. Baturina, and G. E. Wnek, *Electrochem. Solid-State Lett*., 8 (2005) A267.
38. A. T. Haug, and R. E. White, *J. Electrochem. Soc*., 147 (2000) 980.
39. C. Song, L. Zhang, and J. Zhang, *J. Electroanal. Chem*., 58(2006), 293-298.